REPORT DOCUMENTATION PAGE

Form Approved
OMB No. 0704-0188

1. REPORT DATE *(DD-MM-YYYY)*	**2. REPORT TYPE**	**3. DATES COVERED** *(From - To)*
26-06-2013	Final Report	05/01/2010 - 04/30/2013

4. TITLE AND SUBTITLE

HIGH-FIDELITY THERMAL RADIATION MODELS AND MEASUREMENTS FOR HIGH-PRESSURE REACTING LAMINAR AND TURBULENT FLOWS

5a. CONTRACT NUMBER

5b. GRANT NUMBER
FA9550-10-1-0148

5c. PROGRAM ELEMENT NUMBER

6. AUTHOR(S)
Michael F. Modest

5d. PROJECT NUMBER

5e. TASK NUMBER

5f. WORK UNIT NUMBER

7. PERFORMING ORGANIZATION NAME(S) AND ADDRESS(ES)
School of Engineering, University of California, Merced
5200 N. Lake Road Merced, CA 95343

8. PERFORMING ORGANIZATION REPORT NUMBER

9. SPONSORING / MONITORING AGENCY NAME(S) AND ADDRESS(ES)
DFAS LI (800) 756-4571 OPT2 OPT3
27 Arkansas RD
Limestone ME 04751-6216

10. SPONSOR/MONITOR'S ACRONYM(S)
USAF, AFRL

11. SPONSOR/MONITOR'S REPORT NUMBER(S)
F67100

12. DISTRIBUTION / AVAILABILITY STATEMENT
Approval for public release; distribution unlimited.

13. SUPPLEMENTARY NOTES

14. ABSTRACT

The objective of this project was to develop high-fidelity models for radiation and turbulence-radiation interactions (TRI) in high pressure combustion systems with extensive validation of the aforementioned models. New spectral radiation models for combustion gases at elevated pressures, for both conventional and stochastic solution methods, were developed. Several Radiative Transfer Equation (RTE) solution methods were newly designed (development of cell-based as well as stochastic particle-based, line-by-line accurate photon Monte Carlo methods, and formulation and coding of higher-order, 3D spherical harmonics as well as simplified PN schemes). To allow simulation of high-pressure laminar flames required modification of the open source flow code used (OpenFOAM) to include differential diffusion and cell-based stochastic RTE solvers. The models were validated by simulation of laminar high-pressure hydrogen-air flames, as well as turbulent methane-air jet flames.

15. SUBJECT TERMS

combustion, radiative heat transfer, high pressure, simulation

16. SECURITY CLASSIFICATION OF: Approval for public release; distribution unlimited.			**17. LIMITATION OF ABSTRACT**	**18. NUMBER OF PAGES**	**19a. NAME OF RESPONSIBLE PERSON**
a. REPORT	**b. ABSTRACT**	**c. THIS PAGE**	UU	18	Michael Modest, Professor
Unclassified	Unclassified	Unclassified			**19b. TELEPHONE NUMBER** *(include area code)* 209.228.4113

HIGH-FIDELITY THERMAL RADIATION MODELS AND MEASUREMENTS FOR HIGH-PRESSURE REACTING LAMINAR AND TURBULENT FLOWS

Grant Number: FA9550-10-1-0148

Final Report

Michael F. Modest, Shaffer and George Professor of Engineering
School of Engineering, University of California, Merced
Merced, CA 95343

ABSTRACT

The objective of this project was to develop high-fidelity models for radiation and turbulence–radiation interactions (TRI) in high pressure combustion systems with extensive validation of the aforementioned models. New spectral radiation models for combustion gases at elevated pressures, for both conventional and stochastic solution methods, were developed. Several Radiative Transfer Equation (RTE) solution methods were newly designed (development of cell-based as well as stochastic particle-based, line-by-line accurate, photon Monte Carlo methods, and formulation and coding of higher-order, 3D spherical harmonics as well as simplified PN schemes). To allow simulation of high-pressure laminar flames required modification of the open source flow code used (OpenFOAM) to include differential diffusion and cell-based stochastic RTE solvers. The models were validated by simulation of laminar high-pressure hydrogen–air flames, as well as turbulent methane–air jet flames.

SUMMARY/OVERVIEW

It is well-established today that neglecting radiation in atmospheric pressure combustion systems may lead to *overprediction* of temperature of up to 200 °C, while using the usually-employed optically-thin or gray radiation models lead to *underprediction* of up to 100 °C and more [1, 2]. Somewhat less well-known is the fact that, in turbulent combustion systems, there can be strong interactions between turbulence and radiation (TRI). Probability density function (PDF) based calculations have shown that TRI always increases the heat loss from a flame, and that this additional heat loss can reach 60% of the total and more, leading to a reduction in the local gas temperature of 200 °C or more. This is even more true in high-pressure combustors with their larger optical thicknesses [3, 4].

The present research focused on extending the PI's previous work on radiation and TRI in atmospheric pressure systems to the high pressures encountered in modern propulsion systems. The specific objectives were to develop, validate, and apply models for RTE solvers and spectral radi-

ation properties of the most important combustion gases in high-pressure combustion, including the effects of TRI. As a result high-end models for spectral thermal radiation and TRI have been advanced to a level that is more consistent with their importance in chemically reacting flows.

TECHNICAL DISCUSSION

Four specific research areas of this project were: 1) extension of spectral radiation models for combustion gases at the elevated pressures relevant to propulsion systems, 2) extension of efficient and accurate RTE solution methods to high-pressure flames, and 3) perform a systematic and detailed validation of the newly developed models.

Major Achievements

(1) Spectral radiation models for elevated pressures High-fidelity *k*-distribution-based spectral radiation models have been developed for atmospheric pressure combustion [5, 6]. These models have been investigated at the elevated pressures prevalent in propulsion systems. In our current full-spectrum *k*-distribution (FSK) model, *k*-*g* distributions for a mixture are constructed on-the-fly using a high-accuracy database of single-species *k*-distributions together with our narrow-band (NB) mixing model [7]. The NB mixing model [7] assumes that at the NB level the absorption coefficients of gases are uncorrelated (due to their small overlap) and, hence, the transmissivities of gases are multiplicative. At elevated pressure much stronger line overlap is likely and the accuracy of the mixing model needs to be validated. We tested our mixing model for pressures up to 30 bar and our findings are summarized in [8]. Figure 1 shows the absolute errors ($\tau_{\eta,LBL\ direct} - \tau_{\eta,LBL\ mixing}$) in NB transmissivity calculations using our current mixing rule. Since important combustion gases such as CO_2 and H_2O overlap primarily near 2.7 μm, the errors in transmissivity calculations are highest at this spectral location (as shown); everywhere else errors are negligibly small. NB transmissivities calculated using the mixing rule and single-species *k*-distribution databases ($\tau_{\eta,DB\ mixing}$) are essentially identical to LBL-mixing values i.e. $\tau_{\eta,LBL\ mixing}$ (not shown). Although our mixing rule incurs some errors near 3400 cm^{-1}, due to its extremely localized nature it has no significant effect on heat transfer calculations (discussed next).

A 1-D homogeneous isothermal layer of gas mixture (1% CO_2 and 2% H_2O by mole) bounded by cold black walls at various pressures was considered keeping the pressure path length constant at 200 bar.cm. For such a homogeneous medium, the *k*-distribution method is exact and, hence, is expected to yield results within machine accuracy (typically 0.5%). Any error in addition to machine error will be due to our mixing rule to construct mixture *k*-*g*-distribution from individual *k*-*g*-distributions. The nondimensional heat fluxes exiting the medium were calculated using the line-by-line (LBL) , the FSK and more advanced models, such as the multi-scale FSK. The results are tabulated in Table 1. It is seen that errors in heat flux calculations using FSK and MSFSK are always negligibly small compared to the LBL calculations and limited to 1%.

The accuracy of *k*-distribution methods was also investigated for an inhomogeneous medium at high pressure. A 1-D medium containing a CO_2–H_2O–N_2 gas mixture, confined between cold black walls, was considered. The mixture consists of two different homogeneous layers (denoted as left/hot and right/cold layer) adjacent to each other with steps in the temperature and concentrations of the species. Two different total pressures of 1 and 30 bar were considered. The pressure path length of the left/hot layer was kept constant at 60 bar·cm while the same is varied for the right/cold layer. Such problems with steps in species concentration and/or temperature provide an acid test for these methods because of their extreme inhomogeneity gradients. Figure 2 shows the results for the case where the left layer contains 10% CO_2, 20% H_2O, and at 1500 K whereas the right layer contains 20% CO_2, 10% H_2O at 300 K. It is seen that the MSFSK calculations are more accurate

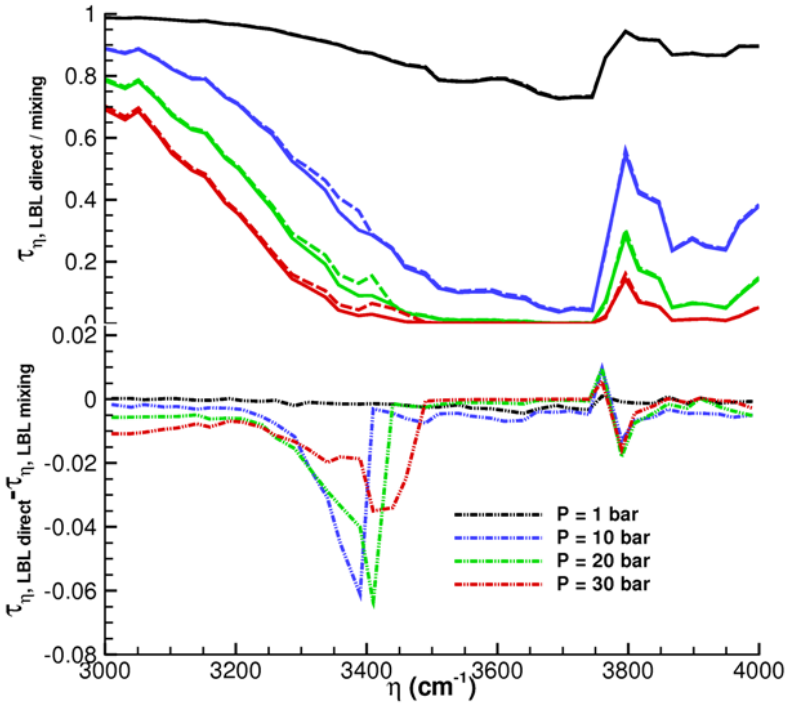

Figure 1: Comparison of NB transmissivities calculated directly and using mixing rule; solid line: direct, dashed line: mixing rule

(approximately by a factor of 4) than the single-scale FSK results for both pressure. Accuracy of both methods increases with increase in pressure.

k-distribution methods were investigated for a more realistic but artificial methane-air flame (from Modest and Zhang [9]) at 30 bar pressure. Temperature and concentration distributions for CO_2, H_2O and CH_4 can be obtained from the previous work of Modest and Zhang [9]. The local radiative heat source term is calculated using LBL, FSK and MSFSK approaches, employing the P_1 method as the RTE solver, and relative errors are determined by comparison with LBL as

$$\text{error}(\%) = \frac{\nabla \cdot q_{\text{LBL}} - \nabla \cdot q_{\text{FSK/MSFSK}}}{\nabla \cdot q_{\text{LBL,max}}} \times 100 \tag{1}$$

The maximum error in local radiative heat source term is 11% using FSK and 2% using MSFSK (see Fig. 3) while their atmospheric counter parts have local maximum errors of 30% using FSK and 7% using MSFSK (see Modest and Zhang [9]).

(2) Extended k-distribution database for elevated pressures The original database of Wang and Modest [10], which employed CDSD-1000 [11] for CO_2 and HITEM$P_1$995 [12] for H_2O, was updated to the latest HITEMP-2010 [13], which includes many million spectral lines activated at high temperature and ensures accuracy up to 4000K. The databased thermodynamic states and narrow-band configurations are summarized in Table 2, covering a wide range of thermodynamic states, larger than the typical ranges a user may encounter in combustion simulations. For example, in a low Mach number combustion simulation, the pressure tends to be almost constant, and only a single (or perhaps very few) pressure values are needed. Similarly, a given combustion application will encounter limited temperature and concentration ranges. Therefore, it is not economical to load the entire database into memory, and for this reason, the current database utilizes dynamic memory management, such that each narrow-band *k*-distribution record is only loaded into memory at the first time it is requested.

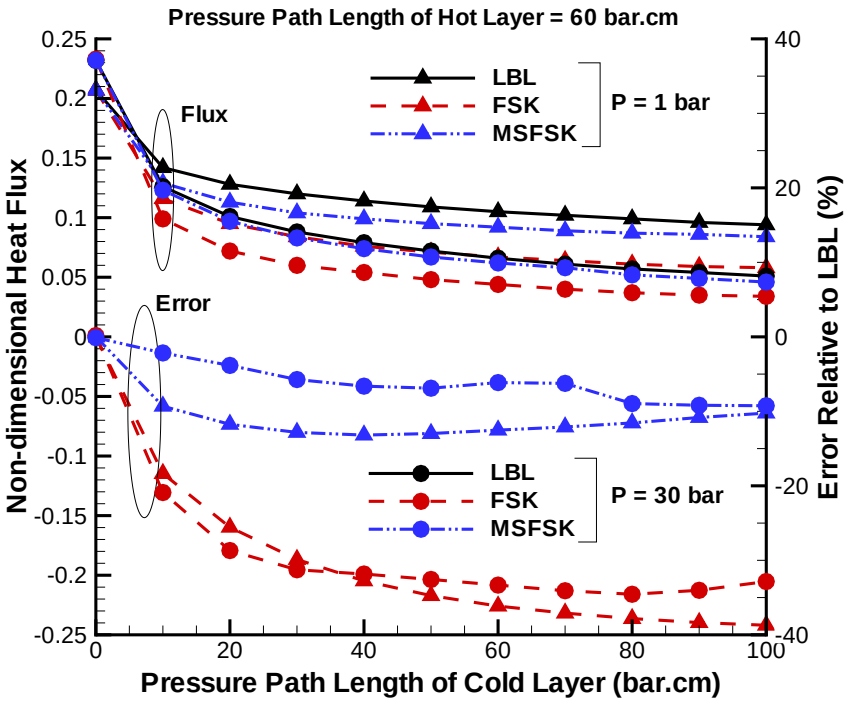

Figure 2: Nondimensional heat flux leaving an inhomogeneous slab at total pressures of 1 and 30 bar, bounded by cold black walls, step changes in mole fraction and temperature: left layer contains 10% CO_2, 20% H_2O, and at 1500 K; right layer contains 20% CO_2, 10% H_2O at 300 K

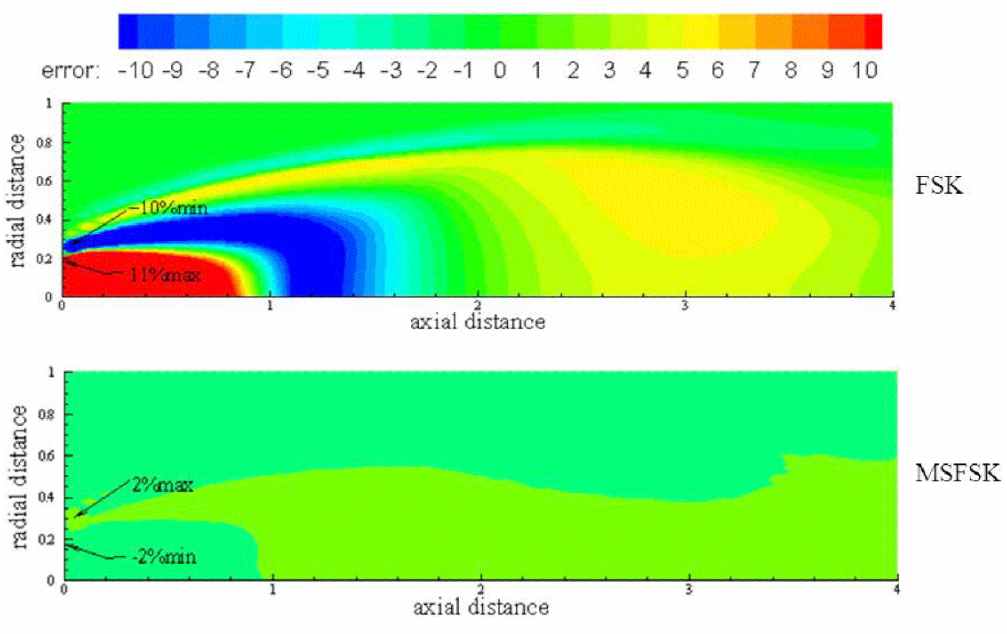

Figure 3: Relative error for radiative heat source calculations using FSK and MSFSK compared to LBL in an artificial 2-D combustion chamber at 30 bar pressure

Table 1: Nondimensional Heat Flux Exiting Homogeneous Isothermal Medium at Various Pressures Using LBL, FSK and MSFSK Methods

T (K)	P×L (bar.cm)	LBL	FSK	MSFSK	Error FSK(%)	Error MSFSK(%)
500	1 bar × 200 cm	0.2134	0.2142	0.2133	0.37	-0.05
	10 bar × 20 cm	0.3325	0.3348	0.3354	0.69	0.87
	20 bar × 10 cm	0.3631	0.3652	0.3662	0.58	0.85
	30 bar × 6.667 cm	0.3916	0.3936	0.3945	0.51	0.76
1000	1 bar × 200 cm	0.1748	0.1748	0.1749	0.01	0.07
	10 bar × 20 cm	0.2338	0.2351	0.2361	0.56	0.98
	20 bar × 10 cm	0.2474	0.2483	0.2499	0.36	1.01
	30 bar × 6.667 cm	0.2551	0.2556	0.2577	0.20	1.00
1500	1 bar × 200 cm	0.1224	0.1227	0.1225	0.27	0.08
	10 bar × 20 cm	0.1486	0.1485	0.1491	-0.07	0.34
	20 bar × 10 cm	0.1538	0.1537	0.1551	-0.70	0.85
	30 bar × 6.667 cm	0.1602	0.1589	0.1618	-0.81	0.98

The accuracy of the narrow-band database was examined by repeating the sample calculations reported for the previous version. Results are similar as before and not shown here. The relative error is maintained to within 1% except for weak lines (mean absorption coefficient below $1 \times 10^{-6}\,\mathrm{bar^{-1}cm^{-1}}$), which is consistent with previous observations.

Differences between the spectroscopy databases are illustrated in Fig. 4. The pressure-based CO_2 absorption coefficient at a temperature of 2000K, pressure of 1bar and the zero mole fraction as calculated from CDSD, HITEM$P_1$995 and HITEMP-2010 are compared. The spectral range of the wavenumbers between 5000 and 5100 $\mathrm{cm^{-1}}$ is shown, which corresponds to the 178th narrow-band of the current database. The narrow-band k-distribution and the corresponding databased values are also compared in Fig. 5. For this particular narrow-band, the absorption coefficients are from HITEMP-2010 are considerably larger than those from CDSD by an approximately fixed value, and this causes the narrow-band k-distribution to shift up by the same amount.

(3) Improved k-distribution model for nonhomogeneous media at elevated pressures

Based on the correlation assumption, there are two methods to find a "correlated-k" value k^*, as shown in Fig.6. It is expected that a reasonable choice of k^* preserves Planck-mean absorption coefficients (i.e., total emission), so that radiative heat sources are accurately predicted at the optically-thin limit. Figure 7 shows the relative error in predicting pressure-based Planck-mean absorption coefficients of CO_2 and H_2O at the pressure of 1 bar and zero concentration limit using the same reference temperature of 1000K but different local temperatures. For both species considered, the previously employed k_{I}^* gives large errors as the local temperature deviates from the reference temperature, while newly proposed k_{II}^* gives relative errors mostly within 1% even when the local temperature deviates from the reference temperature by more than 1000K.

Because an error in predicting the Planck mean absorption coefficient will result in the same amount of error in predicting the radiative heat source in optically-thin conditions as encountered in many laboratory flames, the newly proposed k_{II}^* is more appropriate and suggested.

(4) Improved LBL-accurate photon Monte Carlo method at elevated pressures In order to use a LBL-accurate PMC code, routines had to be generated to find statistically meaningful emission wavelengths for photon bundles that are being traced. With 100s of millions of overlapping spectral lines, finding efficient schemes for this purpose required challenging new models [14–16]. Recently, some improved wavenumber selection schemes have been proposed for hypersonic plasma

Table 2: Precalculated gas states and narrow-bands

Parameter	Sampling	Number of Samples
Species	CO_2, H_2O, CO	3
Pressure (bar)	0.1 – 0.5: every 0.1	5
	0.7:	1
	1.0 – 14.0: every 1.0	14
	15.0 – 80.0: every 5	14
	Total:	34
Temperature	300 – 4000: every 100	38
Mole Fraction	0.0 – 1.0: every 0.25	5
Narrow Band (cm^{-1})	200 – 300: every 10	10
	300 – 4000: every 25	148
	4000 – 5000: every 50	20
	5000 –10000: every 100	50
	10000 –15000: every 250	20
	Total:	248

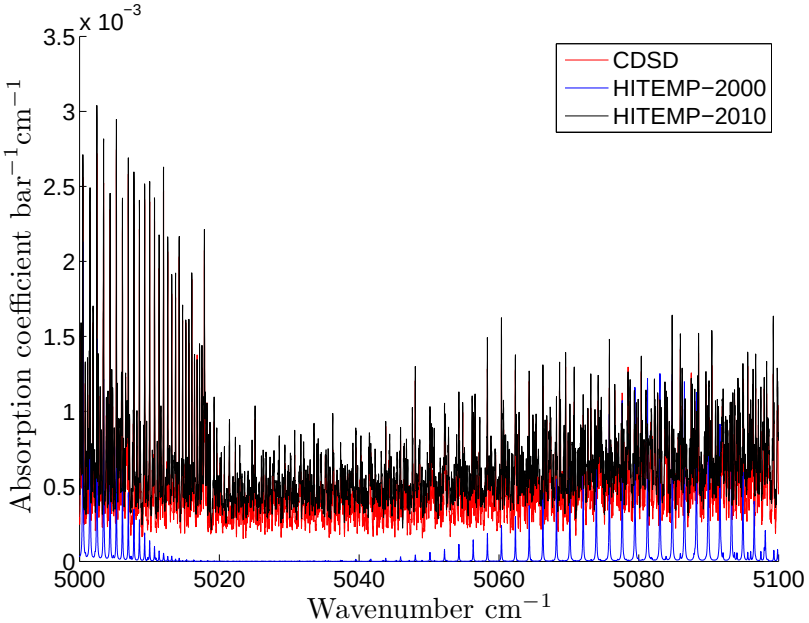

Figure 4: Pressure-based CO_2 absorption coefficients predicted by different spectroscopy databases. Colors are red (CDSD), blue (HITEMP-2000) and black (HITEMP-2010).

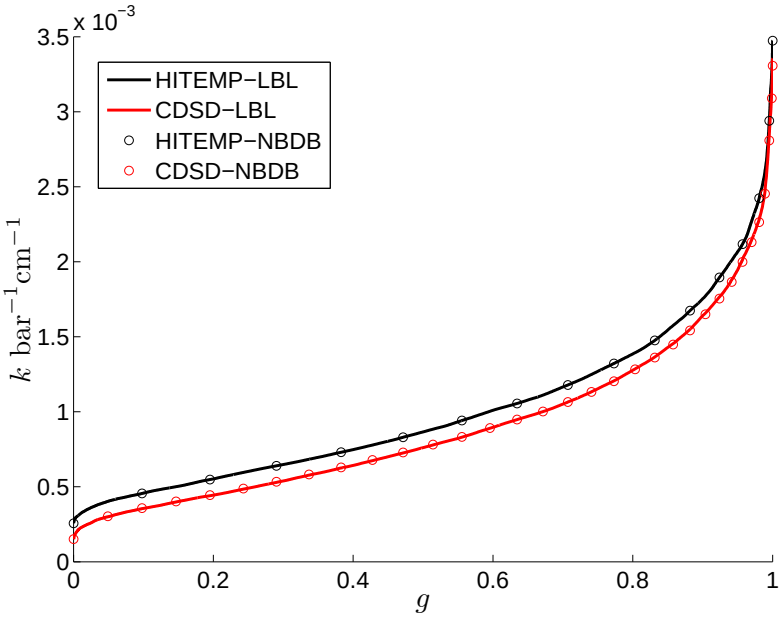

Figure 5: Narrow-band k-distributions calculated from LBL absorption coefficients and their databased values. Lines are LBL calculations, symbols are for narrow-band database. Colors are black (current version) and red (previous version).

radiation in Earth entry applications by Ozawa et al. [17], and by Feldick and Modest [14]. Unlike in combustion and other high-temperature systems, in Earth entry applications, 95% or more of the emitted energy comes from atomic species with very few, but strong, electronic lines. Contribution from diatomic species tend to be minor, and diatomic radiation is due to relatively few rovibrational lines. In their scheme, the rovibrational transition lines were separately databased. However there are too many rovibrational transitions for combustion products such as CO_2, H_2O and CO (several hundred million), making it impractical to database every individual line. By properly applying the improved wavenumber selection scheme to combustion gases, a hybrid scheme was developed for LBL photon Monte Carlo simulations in order to improve efficiency as well as to guarantee accuracy.

In the improved wavenumber selection scheme, emission from different species is considered separately, i.e.,

$$E_{tot} = \sum_{i=1}^{n_s} \int_0^\infty \kappa_{\eta,i} I_{b\eta} \, \mathrm{d}\eta, \tag{2}$$

where $\kappa_{\eta,i}$ is the spectral absorption coefficient of species i, and $I_{b\eta}$ is the blackbody intensity. Emission from individual species is independent from another, i.e., there are no overlap effects for emission. Rather than looking for the appropriate wavenumber for the mixture, one may first determine the emitting species s and then the appropriate wavenumber. Following this idea,

$$R_\eta = \frac{\sum_{i=1}^{s-1} E_i}{E_{tot}} + \frac{\int_0^\eta \kappa_{\eta,s} I_{b\eta} \, \mathrm{d}\eta}{E_{tot}}, \tag{3}$$

where R_η is a random number and s is the number index of the emitting species. E_i is the total

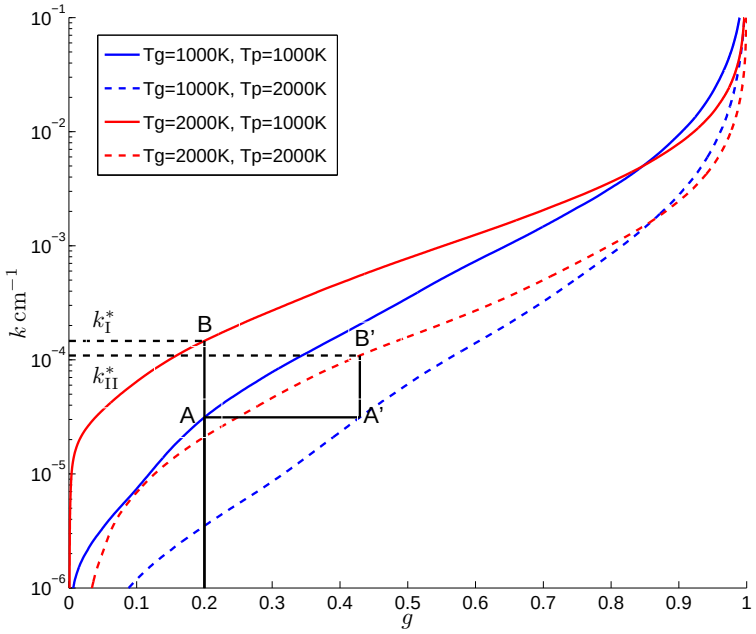

Figure 6: The k-distributions for the evaluation of a "correlated" k^*. Gas composition is 10% H_2O and 90% N_2, and pressure is 1 bar. Colors are blue (gas temperature of 1000 K) and red (gas temperature of 2000K). Lines are solid (Planck function temperature 1000K) and dashed (Planck function temperature 2000K).

emission by species i in the given cell, i.e.,

$$E_i = \int_0^\infty \kappa_{\eta,i} I_{b\eta}\, \mathrm{d}\eta. \tag{4}$$

In the improved wavenumber selection scheme, first a random number for emission wavenumber, R_η, is drawn, and the emitting species s is determined according to

$$s = j \qquad \text{if} \qquad \frac{\sum_{i=1}^{j-1} E_i}{\sum_{i=1}^{n_s} E_i} < R_\eta \leq \frac{\sum_{i=1}^{j} E_i}{\sum_{i=1}^{n_s} E_i}. \tag{5}$$

This ensures that the fraction E_i/E_{tot} of random numbers is employed to pick emission wavenumbers for species i, in accordance with the fractional emission from the species. Once the emitting species is found, R_η is rescaled according to

$$0 \leq R_{\eta,s} = \frac{R_\eta E_{tot} - \sum_{i=1}^{j-1} E_i}{E_j} < 1 \tag{6}$$

By first determining the emitting species s from Eq. (5), an appropriate wavenumber can be found by search through only a single species s. This improved scheme, finding an emitting species explicitly and and emission wavenumber by iteration (in order to eliminate severe interpolation

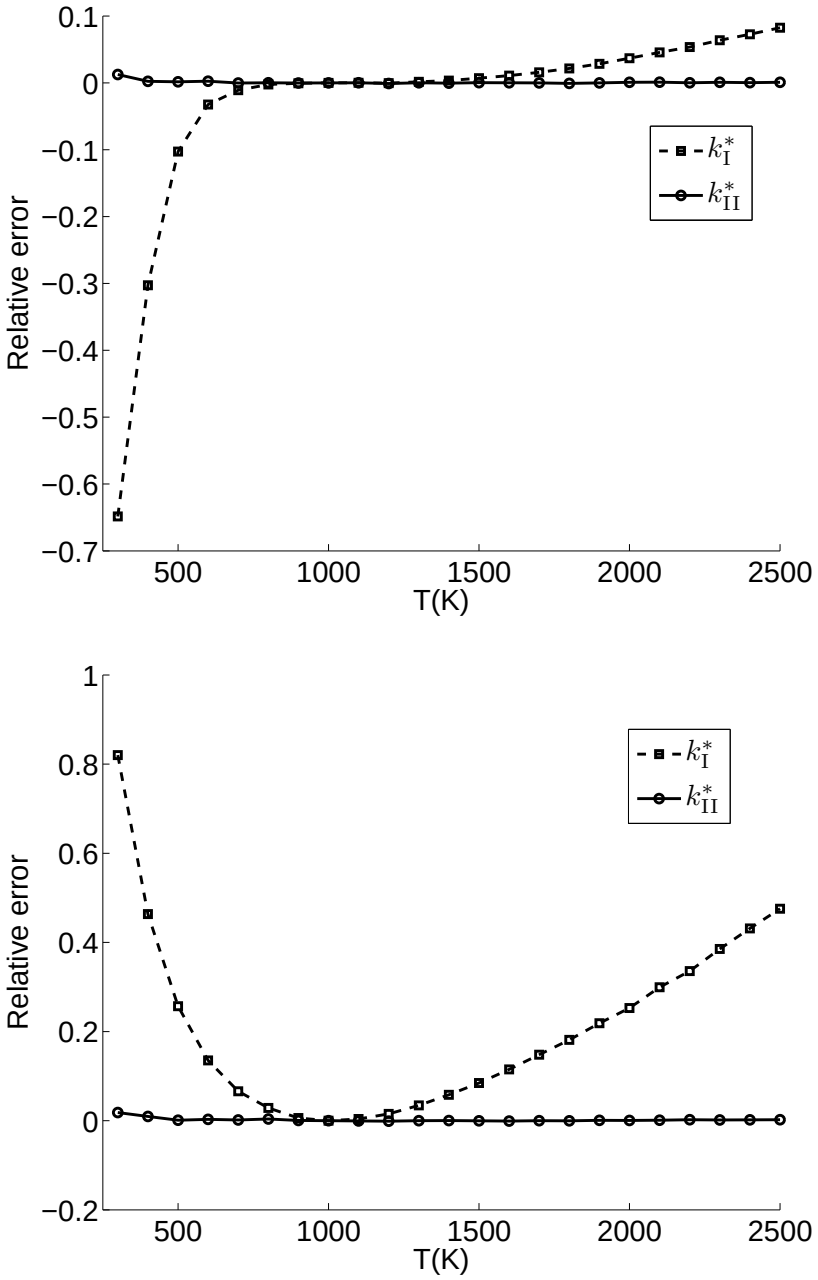

Figure 7: Relative errors in predictions of pressure-based Planck-mean absorption coefficients of CO_2 (top) and H_2O (bottom) at different local temperatures using two k^* schemes. k_{I}^* is for the original evaluation scheme, and k_{II}^* the newly developed method. The reference temperature is 1000K, pressure and mole fraction are 1bar and zero concentration limit for both local and reference states.

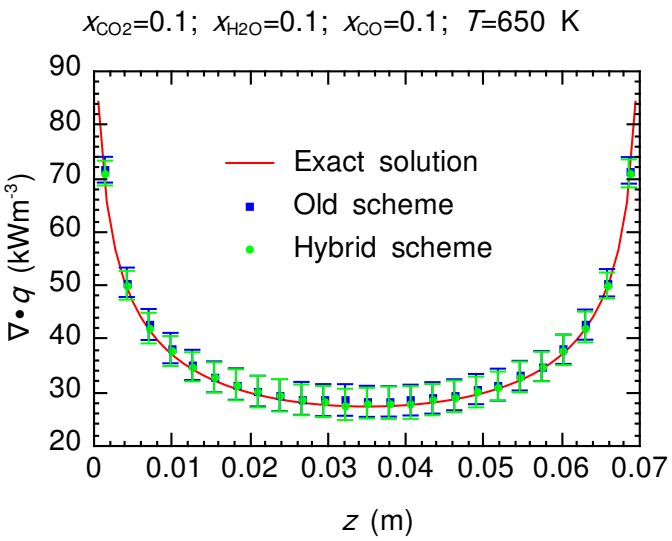

Figure 8: Divergence of radiative flux for 10% CO_2-10%H_2O-10%CO mixture at 650K using the old scheme and the hybrid scheme

errors) is called "hybrid scheme." In this hybrid scheme CPU time for the calculation of mixture random-number relations is reduced by up to a factor of 10.

Accuracy and efficiency of the old scheme and the hybrid scheme incorporated into the PMC model are compared for a one-dimensional example (in the z-direction). The example deals with an isothermal gas at 650K and 1bar contained between two parallel cold black walls. A mixture of 10%CO_2–10%H_2O–10%CO (by mole fraction) and 70% N_2 is investigated, and the resulting divergence of the radiative flux is shown in Fig. 8, comparing results from exact LBL calculations and the old as well as the hybrid emission wavenumber selection schemes. The absorption coefficient data are taken from the HITEMP2010 database in all three cases. It is observed that both Monte Carlo schemes perform equally well, correctly following the LBL solution. Using 10 million photon bundles in the PMC simulation, the hybrid scheme correctly follows the LBL solution, requiring 3.19 s to determine the emission wavenumbers, as opposed to the old scheme, which needed 31.08 s for the identical example; i.e., the computational efficiency for wavenumber selection is improved about by a factor of 10.

(5) OpenFOAM Improvements for Laminar Flames A laminar-diffusion combustion solver, taking into account the effects of differential diffusion, was developed within the open source CFD package OpenFOAM [18]. In addition, OpenFOAM was augmented to take the effect of nonunity Lewis Number into account, which is important in laminar flow. For the diffusion flame solver included in OpenFOAM it is assumed that the Lewis number is unity and the diffusivities of the gas-phase species are equal to either the mixture viscosity or the mixture thermal diffusivity. If the assumption of unity Lewis number is relaxed, an additional term must be added to the energy equation due to enthalpy diffusion. For slow-flowing diffusion flames, the absence of this term can result in large errors, causing unphysical temperature changes even when modeling the mixing of two gases at the same temperature.

For most chemical mechanisms, the system of ODEs is stiff and ODE solvers including SIBS, KRR4 and RK in OpenFOAM have been found to be unstable for stiff systems. Therefore, to compute the chemical source terms, the CVODE stiff ODE solver from the SunDIALS package [19] was incorporated into OpenFOAM, which is able to solve both stiff and non-stiff systems of ODEs.

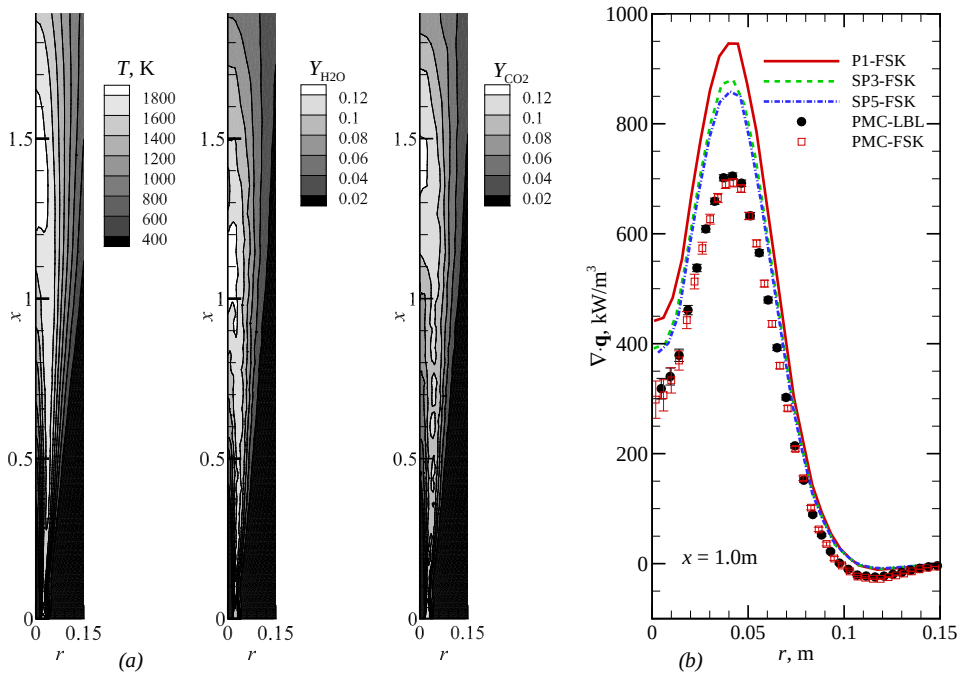

Figure 9: Two-dimensional axisymmetric methane jet flame with variable nongray properties: *(a)* contour maps of temperature and species mass fractions; *(b)* radiative source at fixed axial location ($x = 1.0$ m) as calculated by several methods.

(6) RTE Solver Development To allow for PMC solutions in laminar flames, as well as non-transported PDF turbulent flame simulations, our stochastic particle-based PMC model was modified to allow for cell-based simulations [15]. The new LBL spectral module was attached to both the stochastic-particle and the finite-volume PMC codes. An example of its calculations is given in Fig. 9, depicting the influence of radiation in a time-averaged Sandia D type flow field, scaled up 4 times to make radiation important in such an otherwise laboratory scale flame (a snapshot from a fully converged solution using our stochastic media LBL PMC, and including strong turbulence–radiation interactions). Figure 9a shows temperature and concentration profiles, indicating that CO_2 peaks much farther downstream because of considerable CO formation upstream where water vapor peaks. This puts great demands on the spectral model (making absorption coefficients "uncorrelated"); however, as seen from Fig. 9b, the FSK spectral model when combined with our PMC code gives essentially exact results, i.e., compared to LBL-accurate PMC. The strong gradients (in both temperature and concentrations in both radial and axial directions) also challenge the simple P_1 RTE solver, which incurs errors up to 30%.

To improve the accuracy of conventional RTE solvers, higher-order P_N methods were explored. First, a simplified P_N, or SPN, model was developed, which requires a set of $(N+1)/2$ elliptic P_1 type PDEs, in the hope of improving P_1 accuracy at a reasonable price. The newly developed SPN scheme was successfully tested with a number of 2D problems [20], and results are also included in Fig. 9b. It is seen that maximum errors for SP_3 and SP_5 are reduced to about 20% and 15%, respectively, which is slightly worse than would be expected for the much more complicated and expensive corresponding P_3 and P_5. Radiative heat sources for an artificial turbulent jet diffusion flame (the ubiquitous small Sandia Flame D scaled up 4 times to make radiation more important), employing different models, are presented in Fig. 10. Results from 4 different RTE solvers combined with 3 spectral models are shown. The conventional RTE solvers are paired with various

k-distribution spectral models, and P_1 also with a LBL model; the PMC is always coupled with a LBL spectral method, i.e., provides exact answers for comparison. It is observed that, when coupled with a k-distribution, SP_3 eliminates over 30% of the error for P_1 compared PMC, while SP_5 recovers over one half. The simplified P_N methods require 2 or 3 elliptical equations, respectively, and, therefore, provide relatively cheap improvements over P_1 RTE evaluations. However, when coupled with the Planck-mean gray model, P_1, SP_3 and SP_5 predictions show little difference to the "optically thin" solution (not shown), confirming that spectrally averaged Planck mean absorption coefficients significantly underestimate gas absorption.

CPU costs for k-distribution evaluation of the CO_2 and H_2O mixture per cell is shown in Table 3. The correlation tables require little cpu time. Evaluations using the narrow-band database require much more time because of database interpolation, mixing evaluations for each narrow-band, and assembly of narrow-band to full-spectrum k-distributions. The RTE models, P_1, SP_3 and SP_5 require 0.0312s, 0.125s and 0.172s, respectively, for each quadrature on average. Because SP_3 and SP_5 involve extra iterations between 2 and 3 equations respectively, their time costs are more than 2 and 3 times the P_1 cost, respectively.

Table 3: Time cost (in seconds) for a k-distribution evaluation per cell for a CO_2–H_2O mixture.

	Multiplication	Uncorrelated mixture
correlation tables	0.0016	0.006
narrow-band database	0.0549	0.469

The present calculations are based on a mesh of 3325 cells and an 8 point quadrature scheme for the cumulative k-distribution. The total time for k-distribution assembling was 5.3 and 1560 seconds for the correlation tables mixed with the multiplication model and for the narrow-band database mixed with the uncorrelated mixture model, respectively, which represent computationally the cheapest and the most expensive k-distribution models in the present study. The total CPU time for the RTE solutions is 0.25, 1 and 1.376 seconds for P_1, SP_3 and SP_5, respectively. Since the total computational time is dominated by assembling k-distributions, simplified P_N methods provide relatively cheap improvements over P_1 methods.

Multi-dimensional P_N implementations are mathematically extremely complex [21, 22], resulting in a set of $N(N+1)/2$ simultaneous elliptic PDEs with cross-derivatives. This high-order RTE solution method has also been implemented recently, using built-in operator tools within OpenFOAM. These tools are inadequate for the cross-derivatives required, as well as for simultaneous solution of 6, 15, or more PDEs and, therefore, the present implementation is rather inefficient. The problem is worse for the common axisymmetric problems for which, in theory, only $(N+1)^2/4$ (or 4, 9, ...) PDEs are needed, and which is not exploited by the present implementation. Rather than presenting here the extremely involved mathematics, we show solutions for a cylindrical case to demonstrate P_N solutions for axisymmetric problems. In these types of problems, physical quantities such as temperature, heat flux, intensity, chemical species concentrations, etc., vary only radially and axially, and are considered as 2-D. As a result, for many of these applications, the transport equations are solved over a wedge in order to reduce the computational effort in solving these classes of problems. Here, a full cylinder rather than a wedge is considered in order to demonstrate that the resulting intensity coefficients have azimuthal dependence and, therefore, special care must be taken regarding boundary conditions for general axisymmetric cases. For this example problem, the medium in the cylinder has strongly variable properties with an optical thickness over a diameter at a given height of $\tau_D = 4.5$. Results for incident radiation G and negative radiative source $\nabla \cdot \mathbf{q}$ are shown in Figs. 11(a) and 11(b). An exact solution for this problem is

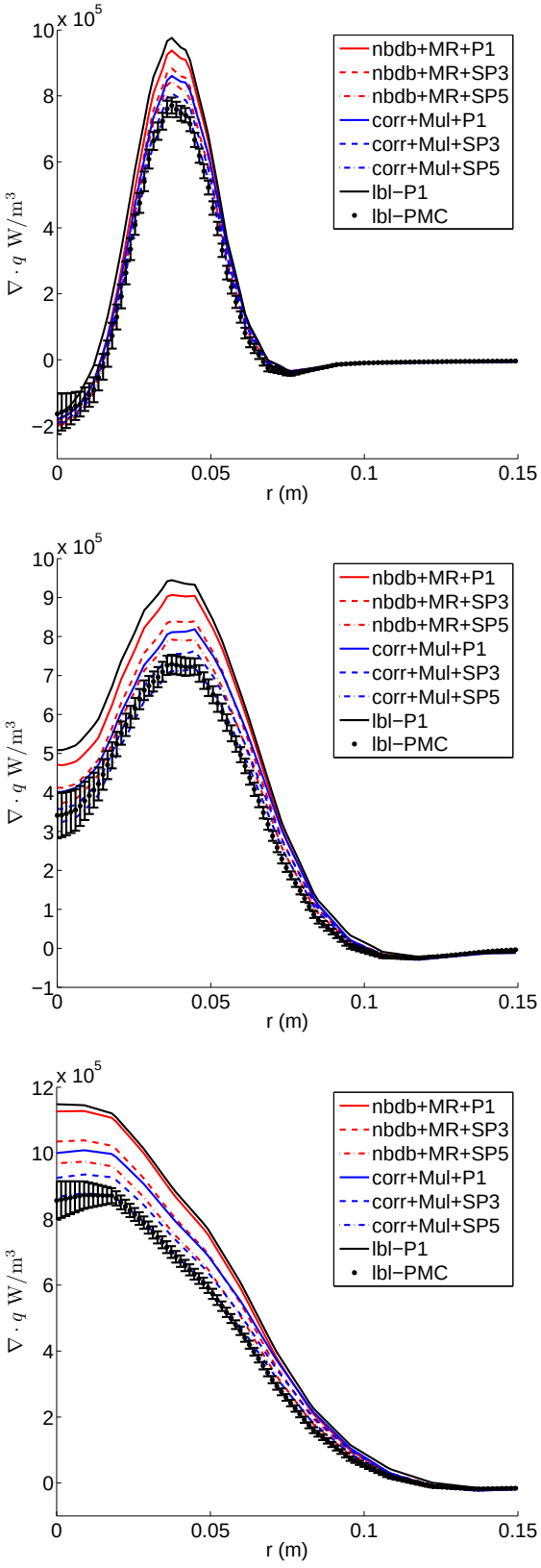

Figure 10: Effects of RTE solvers on radiative heat flux divergence $\nabla \cdot q$ at three downstream locations $y = 0.5$m (top), $y = 1.0$m (middle), and $y = 1.4$m (bottom).

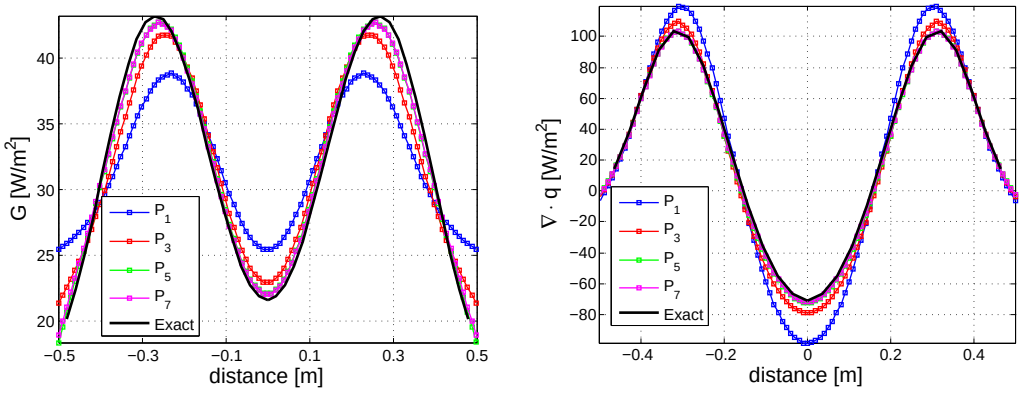

(a) Directional integrated intensity (b) Heat flux

Figure 11: Comparing incident radiation G and divergence of heat flux $\nabla \cdot \mathbf{q}$ computed with higher order P_N for a cylindrical enclosure case. The along the diameter.

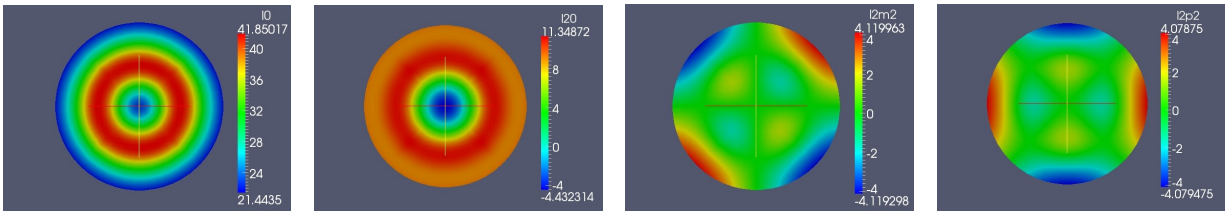

(a) I_0 (b) I_2^0 (c) I_2^{-2} (d) I_2^2

Figure 12: Intensity coefficients of P_3 for cylindrical problem. The resulting fields show that some of the intensity coefficients exhibit azimuthal dependence.

calculated directly from the integral solution of the RTE. The solutions for P_5 and P_7 are close to the exact solution; however, increasing the order of P_N beyond $N = 5$ changes the accuracy very little for this problem. Surface plots of the computed intensity coefficients are shown in Fig. 12. Values of the intensity coefficients I_2^{-1} and I_2^1 are negligible because of the absent variations in the z-direction and, therefore, are not shown. As this figure shows, the intensity coefficients I_2^2 and I_2^{-2} have variations in both the radial r and polar θ directions, whereas I_0^0, has only r dependence as expected. If this problem were to be applied on a wedge, new boundary conditions for I_2^2 and I_2^{-2} must be developed.

While the higher order P_N-approximations have been shown here to be more accurate, they typically require more cpu time. Details regarding the computational effort encountered on the ex-

Table 4: CPU effort on a machine with Processor: Intel Core 2 Duo CPU E8400 3.00GHz × 2. The average cpu time in seconds and the number of inner iterations (M).

Method	1-D slab 60 cells	2-D enclosure 6,889 cells	Cylinder Enclosure 13,520 cells
P_1	< 0.01	≈ 0.01	0.025
P_3	0.16 (8)	6.22 (24)	8.87 (10)
P_5	0.70 (10)	14.79(16)	120.48 (44)
P_7	2.20 (13)	21.76(10)	77.45 (12)

ample problems that were presented here are displayed in Table 4. This table includes the number of interior cells N_c for each mesh, the cpu time, and the number of inner iterations (M). Compared with the numerical experiments from [23], where a 2-D enclosure problem is solved with $N_c = 242$ and the cpu time was reported as < 1s, the application here of P_3 on the 2-D example took 6.22s (an order of magnitude greater) for a much larger N_c (also an order of magnitude greater). Comparing our cpu time results, it appears that P_3 takes at least 2 orders of magnitude longer than P_1, which is considerably more than the minimum factor of 6 (i.e., 6 simultaneous PDEs), due to the presently inefficient OpenFOAM implementation.

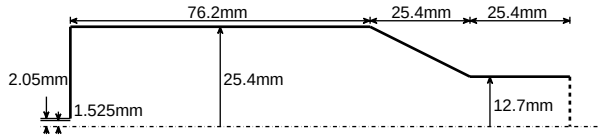

Figure 13: Combustion chamber geometry.

(7) High-Pressure Flame simulations We studied a few high-pressure, laminar hydrogen–air flames numerically, similar to flames, which can be studied experimentally at the Edwards AFB EC-1 facility in future. These flames were studied using both conventional RTE solvers (P_1, SP_3 and SP_5, together with the FSK spectral model), as well as LBL-accurate PMC calculations [15, 24]. The modeled chamber is an axisymmetric version of the EC-1 facility and is shown in Fig. 13. The chamber has a radius of 25.4mm with an exit radius of 12.7mm. The central jet has a diameter of 3.05mm, and an annular jet surrounding it has an inner diameter of 4.1mm. The wall thickness of the inner jet is neglected. The central jet supplies air at a temperature of 300K and a mass flow rate of 0.143g/s. The annular jet supplies hydrogen at a temperature of 300K and a mass flow rate of 4.16×10^{-3}g/s. Simulations were performed for three pressures, viz., 1, 5 and 30 bar. In all three cases, the same mass flow rates are used. Because gas dynamic viscosity has little dependency on pressure, the Reynolds number based on air mass flow rate, viscosity and inner jet diameter is

$$Re = \frac{4\dot{m}}{\pi D \mu} = 3268 \tag{7}$$

for all pressures. This Reynolds number is much lower than the transient Reynolds number of laboratory jet flames, such as Sandia Flames [25] and is expected to result in a laminar flame. The wall temperature is set to 400K. A two-dimensional cylindrical grid with 640 cells is used to discretize all model equations, and is refined near the flame front. Sample results are shown in Fig. 14, showing temperature maps for the 3 different pressures, as calculated without radiation and with radiation, using the simplest P_1/FSK solver. Without radiation, maximum temperature increases with pressure, but at the same time the high-temperature region becomes narrower because of faster reaction rates. Radiative cooling is evident even for the optically thin 1bar flame, becoming stronger at 5bar, and overwhelming at 30bar. This is better seen by looking at a single cross-section (taken to be the chamber exit, giving an indication of the total heat loss from the flame), as shown in Fig. 15: radiation cools down the 1bar flame by roughly 100K (except near the centerline where one sees a temperature increase, caused by downstream absorption), the 5bar flame by 200K, and the 30bar flame by 600K! At 1bar the flame is optically thin, and all RTE solvers return the same result (since there is little self-absorption). Even at higher pressures the differences in results between P_1 and higher-order solvers are small, indicating that P_1 returns accurate results.

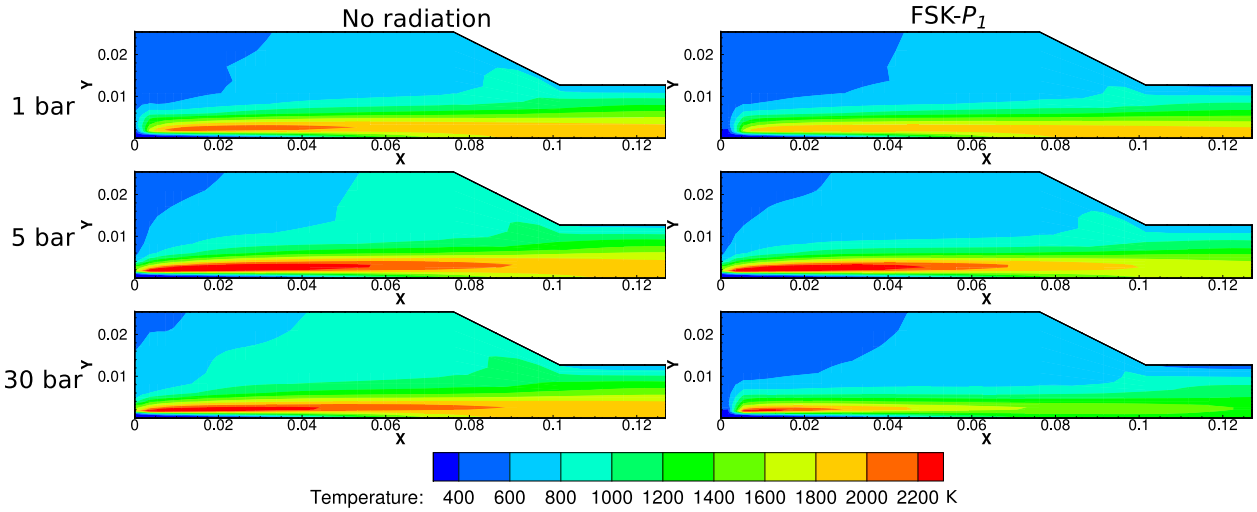

Figure 14: Temperature profiles for laminar model combustor at 3 pressures; left frames: no radiation, right frames: radiation calculated by P_1/FSK model

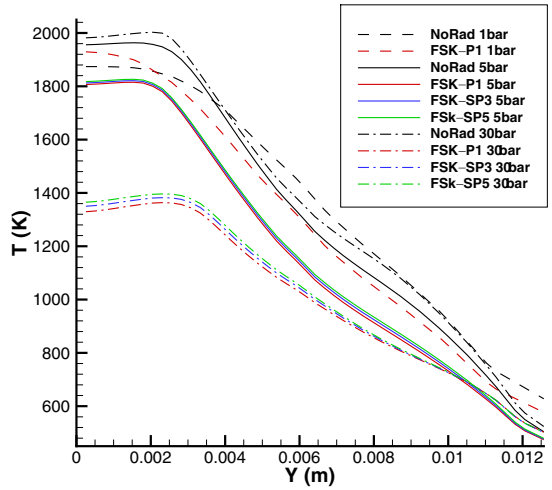

Figure 15: Temperature profiles at the exit cross-section, $x = 0.12$m

REFERENCES

1. L. Wang, D. C. Haworth, S. R. Turns and M. F. Modest, Interactions among soot, thermal radiation, and NOx emissions in oxygen-enriched turbulent nonpremixed flames: a CFD modeling study, *Comb. Flame* 141(1-2) (2005), 170–179.
2. L. Wang, M. F. Modest, D. C. Haworth and S. R. Turns, Modeling Nongray Soot and Gas-Phase Radiation in Luminous Turbulent Nonpremixed Jet Flames, *Comb. Th. Mod.* 9(3) (2005), 479–498.
3. J. B. Moss and C. D. Stewart, Spectrally resolved measurements of radiative heat transfer in a gas turbine combustor, *Experimental Thermal and Fluid Science* 28(6) (2004), 575–583.
4. T. Ebara, N. Iki, S. Takahashi and W. H. Park, Effect of radiation reabsorption on laminar burning velocity of methane premixed flame containing with steam and carbon dioxide, *JSME International Journal Series B—Fluids and Thermal Engineering* 49 (2) (2006), 260–264.
5. G. Pal, A. Gupta, M. F. Modest and D. C. Haworth, Comparison of accuracy and computational expense of radiation models in simulation of nonpremixed turbulent jet flames, In *Proceedings of 2011 ASME/JSME Thermal Engineering Joint Conference*, (2011).
6. G. Pal, A. Gupta, M. F. Modest and D. C. Haworth, Comparison of accuracy and computational expense of radiation models in simulation of nonpremixed turbulent jet flames, *Comb. Flame* (2011), In preparation.
7. M. F. Modest and R. J. Riazzi, Assembly of Full-Spectrum *k*-Distributions from a Narrow-Band Database; Effects of Mixing Gases, Gases and Nongray Absorbing Particles, and Mixtures with Nongray Scatterers in Nongray Enclosures, *J. Quant. Spectrosc. Radiat. Transfer* 90(2) (2005), 169–189.
8. G. Pal and M. F. Modest, *k*-distribution methods for radiation calculations in high pressure combustion, *J. Thermoph. Heat Transfer* (2013), in print.
9. M. F. Modest and H. Zhang, The Full-Spectrum Correlated-*k* Distribution For Thermal Radiation from Molecular Gas–Particulate Mixtures, *J. Heat Transfer* 124(1) (2002), 30–38.
10. L. Wang and M. F. Modest, Narrow-Band Based Multi-Scale Full-Spectrum *k*-Distribution Method for Radiative Transfer in Inhomogeneous Gas Mixtures, *J. Heat Transfer* 127 (2005), 740–748.
11. S. A. Tashkun, V. I. Perevalov, J.-L. Teffo, A. D. Bykov and N. N. Lavrentieva, CDSD-1000, the high-temperature carbon dioxide spectroscopic databank, *J. Quant. Spectrosc. Radiat. Transfer* 82(1–4) (2003), 165–196, available from ftp://ftp.iao.ru/pub/CDSD-1000.
12. L. S. Rothman, C. Camy-Peyret, J.-M. Flaud, R. R. Gamache, A. Goldman, D. Goorvitch, R. L. Hawkins, J. Schroeder, J. E. A. Selby and R. B. Wattson, HITEMP, the High-Temperature Molecular Spectroscopic Database, (2000), available through `http://www.hitran.com`.
13. L. S. Rothman, I. E. Gordon, R. J. Barber, H. Dothe, R. R. Gamache, A. Goldman, V. I. Perevalov, S. A. Tashkun and J. Tennyson, HITEMP, the high-temperature molecular spectroscopic database, *J. Quant. Spectrosc. Radiat. Transfer* 111(15) (2010), 2139–2150.
14. A. M. Feldick and M. F. Modest, An Improved Wavelength Selection Scheme for Monte Carlo Solvers Applied to Hypersonic Plasmas, *J. Quant. Spectrosc. Radiat. Transfer* 112 (2011), 1394–1401.

15. S. Lei, J. Cai, A. Dasgupta, M. F. Modest and D. C. Haworth, Photon Monte Carlo Model for High-Pressure Reacting Laminar Flows, In *Proceedings of IMECE 2012*, No. IMECE2012-88594, ASME, Houston, TX (2012).

16. T. Ren and M. F. Modest, Hybrid wavenumber selection scheme for line-by-line photon Monte Carlo simulations in high-temperature gases, *J. Heat Transfer* (2013), in print.

17. T. Ozawa, M. F. Modest and D. A. Levin, Spectral Module for Photon Monte Carlo Calculations in Hypersonic Nonequilibrium Radiation, *J. Heat Transfer* 132 (2010), 023406.

18. OpenFOAM website, http://www.opencfd.co.uk/openfoam/.

19. A. C. Hindmarsh and R. Serban, User Documentation for CVODE v 2.6.0 (2009).

20. M. F. Modest and S. Lei, Simplified Spherical Harmonics Method For Radiative Heat Transfer, In *Proceedings of Eurotherm Seminar 95*, Elsevier, Nancy, France (April 2012).

21. M. F. Modest and J. Yang, Elliptic PDE formulation and boundary conditions of the spherical harmonics method of arbitrary order for general three-dimensional geometries, *J. Quant. Spectrosc. Radiat. Transfer* 109 (2008), 1641–1666.

22. M. F. Modest, Further developments of the elliptic P_N-Approximation formulation and its boundary conditions, *Numer. Heat Transfer B* 62(2–3) (2012), 181–202.

23. J. Yang and M. F. Modest, High-Order *P-N* Approximation for Radiative Transfer in Arbitrary Geometries, *J. Quant. Spectrosc. Radiat. Transfer* 104(2) (2007), 217–227.

24. J. Cai, S. Lei, A. Dasgupta, M. F. Modest and D. C. Haworth, Radiative heat transfer in high-pressure laminar hydrogen–air diffusion flames using spherical harmonics and k-distributions, In *Proceedings of IMECE 2012*, No. IMECE2012-88507, ASME, Houston, TX (2012).

25. R. S. Barlow and J. H. Frank, Effects of turbulence on species mass fractions in methane/air jet flames, *Proceedings of the Combustion Institute* 27 (1998), 1087–1095.